

Heart Failure Prediction using Modal Decomposition and Masked Autoencoders for Scarce Echocardiography Databases

Andrés Bell-Navas^{a,*}, María Villalba-Orero^{b,c}, Enrique Lara-Pezzi^b, Jesús Garicano-Mena^{a,d}, Soledad Le Clainche^{a,d}

^a*ETSI Aeronáutica y del Espacio, Universidad Politécnica de Madrid, Pl. del Cardenal Cisneros, 3, Madrid, 28040, Spain*

^b*Centro Nacional de Investigaciones Cardiovasculares (CNIC), C. de Melchor Fernández Almagro, 3, Madrid, 28029, Spain*

^c*Departamento de Medicina y Cirugía Animal, Facultad de Veterinaria - Universidad Complutense de Madrid, Av. Puerta de Hierro, Madrid, 28040, Spain*

^d*Center for Computational Simulation (CCS), Boadilla del Monte, 28660, Spain*

Abstract

Heart diseases constitute the main cause of international human defunction. According to the World Health Organization (WHO), approximately 18 million deaths happen each year due to precisely heart diseases. In particular, heart failures (HF) press the healthcare industry to develop systems for their early, rapid, and effective prediction. This work presents an automatic system based on a novel deep learning framework which analyses in real-time echocardiography video sequences for the challenging and more specific task of heart failure time prediction. This system works in two stages. The first one transforms the data from a database of echocardiography video sequences into a machine learning-compatible collection of annotated images which can be used in the training phase of any machine learning-based framework, including a deep learning-based one. This stage includes the use of the Higher Order Dynamic Mode Decomposition (HODMD) algorithm for both data augmentation and feature extraction. The second stage builds and trains

*Corresponding author

Email addresses: a.bell@upm.es (Andrés Bell-Navas), mvorero@ucm.es (María Villalba-Orero), elara@cnic.es (Enrique Lara-Pezzi), jesus.garicano.mena@upm.es (Jesús Garicano-Mena), soledad.leclainche@upm.es (Soledad Le Clainche)

a Vision Transformer (ViT). Self-supervised learning (SSL) methods, so far barely explored in the literature about heart failure prediction, are adopted to effectively train the ViT from scratch, even with scarce databases. The designed neural network analyses images from echocardiography sequences to estimate the time in which a heart failure will happen. The results obtained show the efficacy of the HODMD algorithm and the superiority of the proposed system with respect to several established ViT and Convolutional Neural Network (CNN) architectures. The source code will be incorporated into the next version release of the ModelFLOWS-app software (<https://github.com/modelflows/ModelFLOWS-app>).

Keywords:

Echocardiography Imaging, Heart Failure Time Prediction, Higher Order Dynamic Mode Decomposition, Self-supervised learning, Vision Transformers

1. Introduction

Heart diseases and, in general, cardiovascular diseases (CVDs), are the leading cause of human defunction in the world (Arooj et al. (2022)). A report conducted by the World Health Organization (WHO) shows that nearly 18 million people deceased in 2019 precisely due to CVDs, which supposes around a third of the total defunctions (World Health Organization (1999)). Among these deaths, 85 % were due to heart attacks and strokes. In addition, heart failure (HF) in particular affects around 24 million people worldwide with a median survival of five years (Liu et al. (2023), Valsaraj et al. (2023)). This has become a great economic and social burden which increases over time due to the aging of populations, and which implies demanding resources and high costs in the healthcare system (Valsaraj et al. (2023)). Therefore, early, rapid, and accurate identification and risk assessment of heart failures are of great importance. Moreover, this heart failure prediction is essential for successful timely and cost-effective treatments and to improve the level of life. For heart failure prediction, echocardiography imaging is very widely used, in particular transthoracic echocardiography (TTE). This is because it contains much information about the structure and operation of the heart and, therefore, about the heart state. In addition, it is a non-invasive sophisticated ultrasound method widely available, less costly, rapid, and non-ionizing, boosting low-resource settings and portability. However, several

challenges remain regarding the quality and characteristics of the imaging (e.g., poor contrast, noise). These may hamper interpretation, which must be performed by specialized clinicians.

Over the last years, Artificial Intelligence (AI) has shown to improve welfare and offers great potential to make diagnoses automatic, faster, more accurate, to reduce human errors and costs, and to complement decision-making processes. Considering also the characteristics of echocardiography imaging and this global health crisis, the development of deep learning algorithms applied to echocardiography imaging has become of great interest for heart failure prediction. For example, the work in Valsaraj et al. (2023) adopts the ResNet architecture for a spatio-temporal Convolutional Neural Network (CNN) to predict HF mortality in 1, 3, or 5 years, obtaining accuracies of 81 %, 75 %, and 73 %, respectively, in two private datasets. This work is based on the probability of defunction of patients in each of these timelines with respect to the acquisition date of the echocardiography video. The work considers the following subgroups: healthy, at risk of heart failure (HF), HF with reduced ejection fraction (HFrEF) and HF with preserved ejection fraction (HFpEF). The proposed model demonstrates to be superior to CatBoost gradient boosting based on echo measurements in external validation, i.e., in an independent dataset captured in another country, and so with other characteristics. Specifically, the areas under the receiver-operating curve (AUROC) obtained for the 1-, 3-, and 5-year mortality are 82 %, 82 %, and 78 %, respectively, which are better than the 78%, 73%, and 75% AUROC's obtained with CatBoost. In a similar way, Akerman et al. (2023) utilized a 3D CNN model for the diagnosis of HFpEF in TTE data from 6823 patients, achieving an AUC of 91 %. In Zhang et al. (2018), the proposed CNN automatically measures cardiac structure and function to compute LVEF, which has shown a median absolute difference of 6 % with respect to manual tracings in more than 14 000 echocardiograms. In Behnami et al. (2018), a dual-stream model was proposed for TTE videos from Apical two-chamber (A2C) and four-chamber (A4C) views. The architecture includes shared Recurrent Neural Network layers (RNN) and view-specific feature extraction blocks. This model directly estimates left ventricle ejection fraction (LVEF) without any previous LV segmentation or identification of crucial cardiac frames. Finally, a threshold of 40 % applied on the estimated LVEF value determines either high risk of heart failure (if below the threshold), or low risk (otherwise). The work in Liu et al. (2023) proposes *r2plus1d-Pan*, a deep spatio-temporal convolutional model compatible

with both static and dynamic ultrasound images for the first time, for the diagnosis of HFrEF (i.e., again, EF below 40 %). When trained with these both types of images, the model outperformed most human experts, comprising 15 registered ultrasonographers and cardiologists with different working years in three databases: EchoNet-Dynamic, Cardiac Acquisitions for Multi-structure (CAMUS) dataset, and a local one from the Nacional Cardiovascular Center of China. However, the model results too large, supposing 57.2 GB of file storing.

Some works based on other deep learning techniques estimating the LVEF have also been proposed. For instance, the work in Muhtaseb and Yaqub (2022) combines the advantages of 3D CNNs and Vision Transformers (ViTs) by proposing EchoCoTr, obtaining a Mean Absolute Error of 3.95 in the EchoNet-Dynamic dataset. This result is better than the one obtained in Reynaud et al. (2021) (5.95). Specifically, this work adopts a Transformer architecture based on a residual autoencoder network and on a modified version of the BERT (Bidirectional Encoder Representations from Transformers), acting as a spatio-temporal feature extractor. In parallel, in Fazry et al. (2022), hierarchical ViTs are proposed, with a Mean Absolute Error of 5.59 in the LVEF estimation, without previous LV segmentation.

Among the previously presented works, CNNs are more frequently used for heart failure prediction (Petmezas et al. (2024)), and this is based on determining their grade of risk (e.g., via the EF, like in Behnami et al. (2018)) or estimating the probability of mortality in a standard timeline, for example, like in Valsaraj et al. (2023). On the other hand, these works do not perform adaptations to deal with database scarcity, common in the medicine field.

The present contribution proposes a different data-driven solution, based on deep learning methods, to address the more specific task of estimating the concrete age of patients in which heart failures will happen. To the best of the authors' knowledge, this more challenging task has not been addressed in the related literature. A novel procedure has been devised to create a large database from different sources of echocardiography images with heart failure prognoses provided by human experts. One of the main purposes for this database creation process is to improve the discriminating capability of standardized neural network architectures in the usual scenario of having a scarce number of samples. Precisely, in the medicine field, the difficulty resides in obtaining a varied database of echocardiography images with high quality for an adequate training of deep learning algorithms. This is because very hard specialized work with specific knowledge about heart diseases and failures is

required, implying high costs. In addition, these sources of echocardiography images are heterogeneous regarding the image resolution and frame rate, due to different acquisition conditions and sensors used. Therefore, it is not possible to use them simultaneously to create a larger database. The proposed procedure enables the homogenization of the different sources of echocardiography images to create a larger database required by the proposed deep learning algorithm, again, contributing to performance improvements. This also includes the use of a data-driven method, the Higher Order Dynamic Mode Decomposition (HODMD) (Le Clainche and Vega (2017)). Its purpose is to generate images with less noise and more discriminative features than the original data (with high noise by nature), associated with the different cardiac conditions, thus augmenting the training database, and improving the heart failure prediction accuracy. Moreover, the HODMD modes contain temporal information, extracted from the sequences, which could be relevant to characterize different heart states and more accurately predict heart failures. Regarding the proposed deep neural network, it incorporates training mechanisms based on self-supervised learning (SSL) to palliate the usual need for large databases, especially in ViTs (Lee et al. (2021)), further addressing the difficulty to gather large high-quality databases in the medicine field. The adoption of self-supervised learning, even less the use of Masked Autoencoders (MAE) (He et al. (2022)), has been barely explored in the related literature about heart failure prediction in echocardiography images to the best of the authors' knowledge. As a result, the proposed system can automatically estimate the age in which a heart failure will happen from echocardiography video sequences without the intervention of human experts during its operation. In addition, that estimation can be performed in real-time. Therefore, the proposed system addresses the heart failure prediction task as a regression problem. That is, given a test sample, this system estimates a real value of the time of heart failure, instead of classifying between a set of classes. This is different to the usual approach of classifying in either a general level of risk of heart failure (i.e., low, high) or in a standard timeline, instead of estimating a concrete time of heart failure.

This work largely extends the preliminary studies carried out in Groun et al. (2025), Bell-Navas et al. (2023), and Bell-Navas et al. (2024) by proposing the new database creation procedure, the deep learning architecture, and giving experimental results about the heart failure prediction performance. The source code used in this work will be incorporated into the next version release of the ModelFLOWs-app software (Hetherington et al. (2024)).

The organization of the paper is as follows. Section 2 describes the proposed heart failure prediction system. Section 3 introduces the database created to assess the proposed system. Section 4 summarizes the obtained results with the proposed system and makes a comparison with other algorithms. Finally, conclusions are drawn in Section 5.

2. Heart Failure Prediction System

The heart failure prediction system here proposed is aimed to analyse echocardiography images using an adapted deep neural network architecture to predict the time of happening a heart failure in real-time. This neural network is based on a ViT that introduces training mechanisms from self-supervised learning to palliate the need for large databases. This fact allows to effectively train the ViT from scratch, even with scarce datasets. The system output is the prediction of the time of happening a heart failure from the input sequence of echocardiography images. The heart failure prediction system has been carefully trained using a new and large cardiac database, whose creation is a key contribution of this paper. This cardiac database creation comprises a multi-stage procedure applied to sequences of echocardiography images showing hearts with different states and pathologies. Each of these sequences also includes an annotation of the time in which a heart failure happens, provided by doctors. The designed procedure generates a machine learning-compatible cardiac database, addressing the fact that the echocardiography images have been acquired with different sensors. Thus, they have different characteristics (image resolution and frame rate, among others). Therefore, it also alleviates the need to collect large databases required by ViTs (Lee et al. (2021)), as this results very expensive in the medicine field, supposing much effort for experts.

Fig. 1 depicts the block diagram of the proposed heart failure prediction system, divided into two major stages: Cardiac Database Creation, and Heart Failure Prediction; those are described in detail in the next subsections.

2.1. Cardiac Database Creation

This stage is aimed to create a large annotated database from echocardiography images acquired with different sensors. The input consists of a heterogeneous collection of sequences of echocardiography images with additional medical information. Each sequence has the diagnosis of the heart

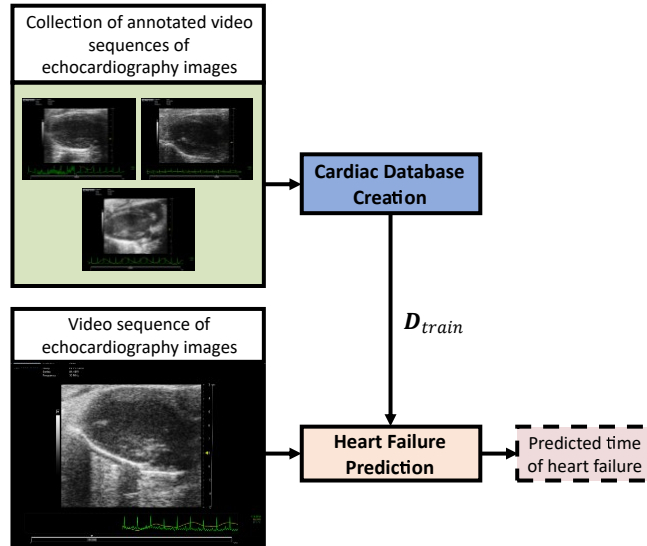


Figure 1: Block diagram of the proposed heart failure prediction system, with representations of echocardiography images with non-heart regions (i.e., the electrocardiogram, medical information, and the black background).

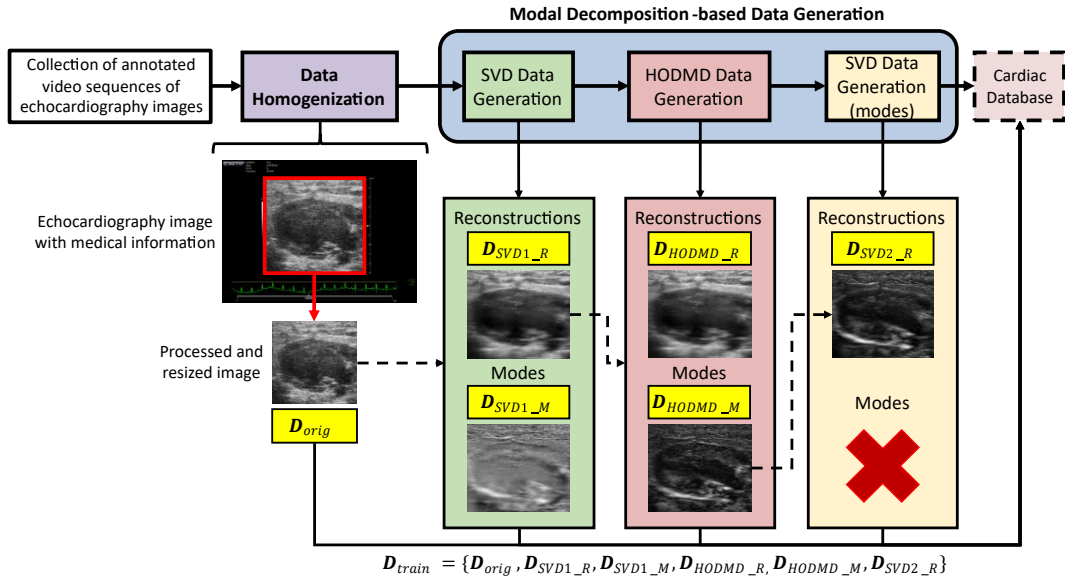


Figure 2: Block diagram of the Cardiac Database Creation stage, composed of two phases: Data Homogenization, and Modal Decomposition-based Data Generation.

state, and the time of happening a heart failure, made by doctors. The output of this stage is a database composed of samples (as images) representing different heart states with homogenized spatial and temporal characteristics, adjusted to a target acquisition device. In this way, the resulting database can be used by machine learning algorithms. This Cardiac Database Creation stage can be further divided into two phases (see Fig. 2): 1) Data Homogenization, and 2) Modal Decomposition-based Data Generation.

The first phase, Data Homogenization, extracts the region representing the heart from the original images of the sequences. All areas outside this region are discarded (containing medical information and the black background). This is accomplished with edge detection algorithms which locate the boundaries of the area corresponding to the echocardiography image itself (i.e., the region containing the heart).

In the second and last phase, Modal Decomposition-based Data Generation, novel samples are generated from the resulting homogenized sequences, denoted as \mathbf{D}_{orig} . These novel samples consist of images with more discriminative features than those of the original echocardiography data. This generation is performed by sequentially applying the Singular Value Decomposition (SVD) (Sirovich (1987)) and the HODMD algorithms (Le Clainche and Vega (2017), Groun et al. (2022)) to each homogenized sequence and taking the outputs of each algorithm. This phase can be seen as a machine learning method based on data physics, in which data augmentation with modal decomposition is performed. Conventional data augmentation techniques based on geometric transformations have also been applied, as will be specified in Subsection 2.2, complementing this data augmentation based on modal decomposition. However, these conventional techniques are not based on physics and only explore slight variations of the actual samples. Therefore, these do not generate discriminative features which strengthen the differentiation between the heart states and better identify heart failures, so the conventional data augmentation techniques used barely lead to performance improvements.

The steps performed in the Modal Decomposition-based Data Generation phase are as follows. First, the SVD algorithm is employed using the homogenized sequences (i.e., \mathbf{D}_{orig}). This generates a series of modes (\mathbf{D}_{SVD1-M}) and the reconstructions of the echocardiography images (\mathbf{D}_{SVD1-R}). Next, the HODMD algorithm is applied to these reconstructions obtained with the previous SVD algorithm, that is, on \mathbf{D}_{SVD1-R} . As a result, HODMD modes and reconstructions associated with the sequence are obtained, represented

as \mathbf{D}_{HODMD_M} and \mathbf{D}_{HODMD_R} , respectively. Subsubsection 2.1.1 describes in more detail the HODMD algorithm for feature extraction and data augmentation. Finally, the SVD algorithm is applied to the HODMD modes (\mathbf{D}_{HODMD_R}), obtaining SVD modes associated with the HODMD modes and their reconstructions. From the data obtained in this latest use of the SVD algorithm, only the reconstructions of the HODMD modes are considered (\mathbf{D}_{SVD2_R}), and the modes are discarded. Note that a sequence must cover a number of heart cycles enough to be able to apply the HODMD algorithm and, therefore, the subsequent SVD algorithm. In this way, the temporal information is correctly characterized, and fair reconstructions can be obtained. This is achieved by applying a threshold which indicates the minimum number of snapshots required in a sequence to apply the HODMD algorithm. Note that the reconstructions are leveraged due to having less noise than their associated original data, making the patterns of the different heart pathologies more distinct. In fact, original echocardiography imaging is typically afflicted by noise. Therefore, the SVD and HODMD algorithms further contribute to the extraction of discriminative features due to also effectively reducing noise as one of their main roles, improving the final heart failure prediction performance. In addition, the deep neural network can potentially learn better the temporal information of the sequences with the use of the obtained HODMD modes and their associated reconstructions (obtained with the second use of the SVD algorithm). This is because the HODMD modes describe the physical patterns associated with the dynamics of the data. These physical patterns can be related to heart diseases (Groun et al. (2022)).

As a result, an annotated cardiac database with a large number of samples is obtained, whose spatial and temporal characteristics are adjusted to the target sensor used in the proposed heart failure prediction system. This is used as a training database \mathbf{D}_{train} to learn a deep neural model, which is the core of the Heart Failure Prediction stage described in Subsection 2.2. Table 2 summarizes the different combinations of the data generated by the SVD and HODMD algorithms (that is, \mathbf{D}_{SVD1_M} , \mathbf{D}_{SVD1_R} , \mathbf{D}_{HODMD_M} , \mathbf{D}_{HODMD_R} , and \mathbf{D}_{SVD2_R}) which are taken to form \mathbf{D}_{train} . This table will be presented and described in more detail in Section 3. Precisely, the combinations with HODMD modes and reconstructions of the echocardiography images lead to the best results, because of having more samples and also more discriminative features derived from modal decomposition.

2.1.1. Higher Order Dynamic Mode Decomposition

The Higher Order Dynamic Mode Decomposition algorithm (HODMD) (Le Clainche and Vega (2017)) is an extension of the Dynamic Mode Decomposition (DMD) (Schmid (2010)), widely used in fluid dynamics and for diverse industrial applications (Groun et al. (2022), Vega and Le Clainche (2021)). HODMD decomposes spatio-temporal data (in this case, a video sequence of echocardiography images) into a number of DMD modes. Each one is associated with a frequency, a growth rate, and an amplitude. The most important modes represent the most discriminative patterns associated with the different heart states in echocardiography images, leading to more accurate heart failure predictions. Specifically, according to Groun et al. (2022), these most relevant modes are typically associated with the highest amplitudes. This decomposition also allows to identify and filter out noisy modes, which, in turn, tend to be those associated with small amplitudes (i.e., a_m in Eq. 2 below). In particular, these consist in high frequencies related to the high noise inherent to the echocardiography imaging, which, therefore, do not contain relevant features of the data and of the heart states. In this way, reconstructions of each frame from the input sequence could be obtained, with less noise and with more discriminative features associated with the different heart states. The HODMD algorithm used in this work is specifically the multidimensional iterative HODMD algorithm (Le Clainche et al. (2017), Groun et al. (2022)). It is based on the Higher Order Singular Value Decomposition (HOSVD) (Tucker (1966)), which extends the SVD algorithm by applying it along each spatial dimension to better clean the data.

Fig. 3 depicts the steps performed by the HODMD algorithm on a sequence of echocardiography images, which are as follows. Assuming that the sequence has been homogenized as described in Subsection 2.1, each frame (or snapshot) is reshaped into a vector of dimensions $N_p = N_x \times N_y$, where N_x and N_y denote the spatial resolution of the snapshots, and N_p the number of pixels of the snapshot. Once all vectors have been computed, a tensor is formed. The dimensions of the tensor are $N_p \times K$, where K is the number of snapshots of the sequence. Then, a dimensionality reduction is carried out by applying the HOSVD algorithm. After that, a decomposition in eigenvalues and in eigenvectors is conducted. In this case, a number of d subsequent snapshots is considered as a contribution given by the HODMD algorithm to improve the precision.

For this purpose, the higher order Koopman assumption is applied, which

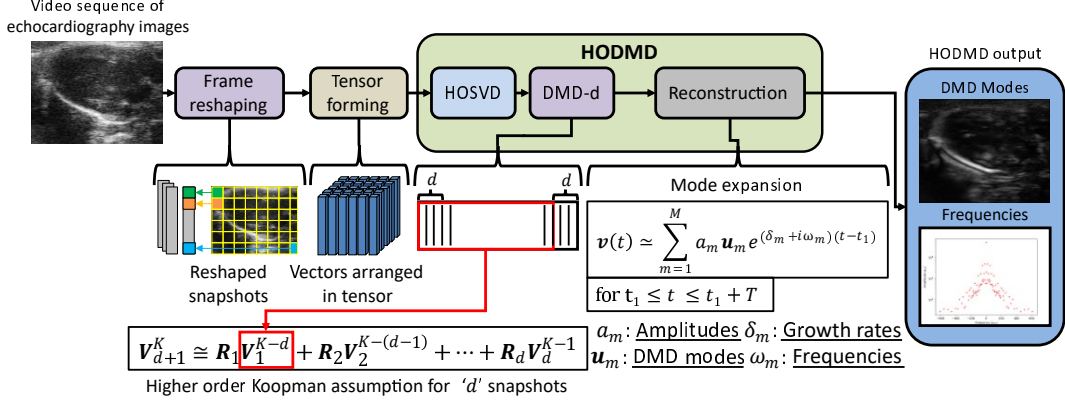


Figure 3: Block diagram of the HODMD algorithm applied on a video sequence of echocardiography images.

relates an echocardiography image with their d previous snapshots with the following expression:

$$\mathbf{V}_{d+1}^K \cong \mathbf{R}_1 \mathbf{V}_1^{K-d} + \mathbf{R}_2 \mathbf{V}_2^{K-(d-1)} + \dots + \mathbf{R}_d \mathbf{V}_d^{K-1}, \quad (1)$$

where \mathbf{V}_{d+1}^K represents the measurement of the image one time step into the future, related with their d previous K equispaced snapshots by the \mathbf{R}_i Koopman operators. Next, the DMD modes \mathbf{u}_m are computed. Finally, a mode expansion process is performed, obtaining the frequencies, the growth rates, and the amplitudes, using the following expression:

$$\mathbf{v}(t) \simeq \sum_{m=1}^M a_m \mathbf{u}_m e^{\delta_m + i\omega_m(t-t_1)} \quad \text{for } t_1 \leq t \leq t_1 + T, \quad (2)$$

where $\mathbf{v}(t)$ represents the spatio-temporal data (i.e., the sequence of echocardiography images) as an expansion of M DMD modes; t is the time, T the sampled timespan, a_m the (real) amplitudes, \mathbf{u}_m the normalized spatial modes, δ_m the growth rates, and ω_m the frequencies. The Koopman operator (Le Clainche and Vega (2017)) allows to relate measurements from a non-linear system (in this case, echocardiography images) in consecutive time steps with a linear operator of infinite dimension. This means that the HODMD algorithm, although formulated with linear operators, as an approximation of the Koopman operator, can deal with the non-linearity which could be present in the echocardiography imaging. All these steps are applied

iteratively until the number of HOSVD modes converges, i.e., remains the same. The DMD modes allow to eventually reconstruct each snapshot (each frame) from the input sequence.

Among the obtained DMD modes, only the most representative ones are selected for the feature extraction and data augmentation. These representative modes are those containing characteristic patterns associated with the different heart states which improve the heart failure prediction. The selection of modes is performed by first comparing their associated frequencies with those which are characteristic of the different heart states, previously identified with the HODMD algorithm in Groun et al. (2022). The frequencies related to the different heart states are those associated with higher amplitudes. Therefore, their corresponding DMD modes describe the physical patterns associated with the dynamics of the echocardiography imaging. In this way, the modes with higher amplitudes, and with frequencies more similar to those of the heart states (identified in Groun et al. (2022)) are taken. These modes with higher amplitudes retained are in turn associated with a tolerance (previously configured for the HODMD algorithm). Regarding the other modes, which tend to have higher frequencies and smaller amplitudes, are associated with the noise of the echocardiography imaging, and so these are discarded. The most representative DMD modes, together with the reconstructions, can be leveraged by the deep neural network to improve the heart failure prediction performance.

2.2. Heart Failure Prediction

The Heart Failure Prediction stage predicts the times of happening heart failures from the corresponding input echocardiography images in real-time. Specifically, the input is a sequence of echocardiography images obtained by medical devices. It is adapted to the target acquisition device used in production in the previous Cardiac Database Creation Stage. The output of the Heart Failure Prediction stage is the estimated age of the corresponding patient in which a heart failure will happen.

The Heart Failure Prediction stage can be divided into four phases, as shown in Fig. 4: 1) Data Homogenization, 2) Modal Decomposition-based Data Transform, 3) Deep Neural Network-based Heart Failure Prediction, and 4) Fusion of Heart Failure Predictions. In the first phase, Data Homogenization, the input sequence is homogenized as already described in Subsection 2.1.

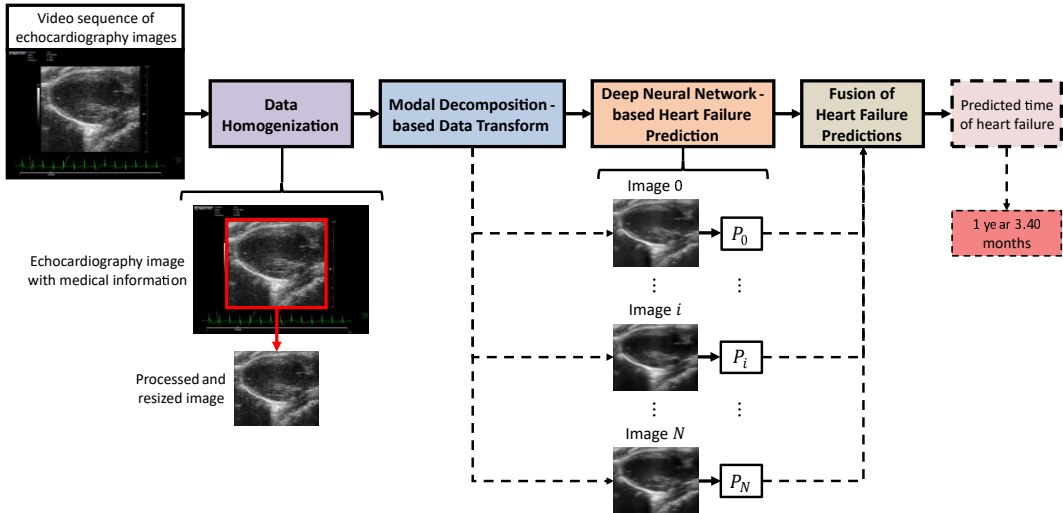


Figure 4: Block diagram of the Heart Failure Prediction stage.

In the second phase, Modal Decomposition-based Data Transform, the same process as in the Modal Decomposition-based Data Generation phase described in Subsection 2.1 is performed. This is, images with less noise and more discriminative features than the original echocardiography data are obtained by sequentially applying the SVD and the HODMD algorithms in the same way as previously described, increasing the differentiation between the heart states and improving the heart failure prediction performance. Therefore, this phase only acts as a feature extractor. However, unlike the Modal Decomposition-based Data Generation phase described in Subsection 2.1, the resulting images from this phase, Modal Decomposition-based Data Transform, are taken as input of the deep neural network for the prediction of the time of a heart failure of the corresponding sequence. On the other hand, the Modal Decomposition-based Data Generation phase leverages the output of each applied algorithm to enlarge the training database and form \mathbf{D}_{train} , directly fed to the deep neural network for training, containing more discriminative samples for the differentiation between the heart states, and addressing the limited availability of high-quality samples usual in the medicine field. Different types of data resulting from the Modal Decomposition-based Data Transform phase have been tested as input of the deep neural network for the prediction of heart failure times in Section 4: the original echocardiography images (that is, without the Modal Decomposition-based Data

Transform), the reconstructions, or modes obtained after applying the SVD or the HODMD algorithm. In particular, according to the results (see Section 4), adopting HODMD data from the test video sequences of echocardiography images as the output of the Modal Decomposition-based Data Transform phase tends to give better heart failure time prediction performances. This demonstrates the efficacy of these techniques to extract more discriminative features associated with the different heart states from echocardiography images and to filter out the high noise inherent, leading to more accurate heart failure time predictions.

The third phase, Deep Neural Network-based Heart Failure Prediction, computes the heart failure time prediction for each image generated in the previous phase, Modal Decomposition-based Data Transform. For this purpose, a deep neural network architecture based on the ViT is used. It has been trained using a self-supervised learning approach which improves the heart failure time prediction performance, even with scarce datasets (Das et al. (2024)). To the best of the authors’ knowledge, self-supervised learning has been barely explored in the related literature about heart failure prediction in echocardiography images, even less Masked Autoencoders (MAE) (He et al. (2022)). Moreover, standard architectures have been proposed as the general trend with no specific adaptations nor approaches to deal with this typical scenario in the medicine field of having a low number of high-quality samples. The training approach used involves two tasks: the Self-supervised Auxiliary Task, which aids in training the ViT for the regression task about heart failure time prediction, precisely the one of interest. This allows to increase the locality inductive bias of the ViT, and so to improve the performance on heart failure prediction in the usual scenario of scarce datasets. In addition, this training approach further reduces the dependence on very large training databases with high quality, which are costly to elaborate and which require much hard specialized work. As will be seen in Subsection 4.2, the proposed deep neural network trained with this self-supervised learning approach achieves a better performance than several ViT architectures and Convolutional Neural Networks (CNN), allowing to reduce computational resources.

The architecture is represented in Fig. 5. Two tasks are jointly learned at the same time: the Self-supervised Auxiliary Task (Fig. 5 (b)), and the Regression Task (Fig. 5 (c)). The first one is aimed to reconstruct the missing patches from masked images, improving the discriminating capability of the deep neural network aimed to predict heart failure times, i.e., the one devoted

to the Regression Task. Precisely, the weights of the Transformer Encoders used for both tasks are shared (highlighted in red in Fig. 5), allowing this joint training. Note that any self-supervised learning approach can be used, but the Masked Autoencoder (MAE) (He et al. (2022)) has been employed due to its popularity and superior performance (Das et al. (2024)). This training approach based on joint learning is different to the usual approach adopted in MAEs (He et al. (2022)), which first performs the pretraining of the ViT for reconstruction of the masked patches, and then the fine-tuning, using the same dataset, for the task of interest. This different training approach not only improves the discriminating capability and feature learning of the deep neural network, but also allows to speed up the training process by learning both tasks at the same time. The common input for the two tasks is an image representing a heart in a determined state (Fig. 5 (a)). As a result of the previous phase, Modal Decomposition-based Data Transform, this input image can be a reconstruction, or a mode obtained with the SVD and the HODMD algorithms. This fact gives the deep neural network the advantage of being able to directly use images as input, in the form of original echocardiography data, reconstructions, or modes obtained with the modal decomposition techniques. However, as said previously, using data obtained with the HODMD algorithm as input for the deep neural network (and so as the output of the Modal Decomposition-based Data Transform) has led to the best performance. The output is a prediction which represents the estimated time in which a heart failure will happen (Fig. 5 (d)). The ViT, as a deep neural network, is the one which addresses the non-linear relationships which could be present between the input and the output, in this case, between echocardiography images and heart failure times, regardless of whether the SVD and the HODMD algorithms have been employed or not. However, as will be seen in Section 4, the use of the SVD and HODMD algorithms for both feature extraction and data augmentation, and the fact that the proposed ViT is specifically adapted to scarce databases of echocardiography images, allow this proposed deep neural network to effectively model the relationship existing between echocardiography images and heart failure times. In addition, as already seen in Subsubsection 2.1.1, the HODMD algorithm, formulated with linear operators, is an approximation of the Koopman operator, allowing to deal with the non-linearities existing in the echocardiography imaging.

The processing of the input (Fig. 5 (a)) for the Regression Task (the one of interest, Fig. 5 (c)), for heart failure time prediction (Fig. 5 (d)) closely

follows the standard ViT architecture. That is, a division in non-overlapping patches is firstly performed. Next, the spatial dimension of the patches is flattened, followed by a normalization layer and a linear projection. Before processing the patches with the Transformer Encoder, positional information and a regression token, with a similar role to the class token, are added.

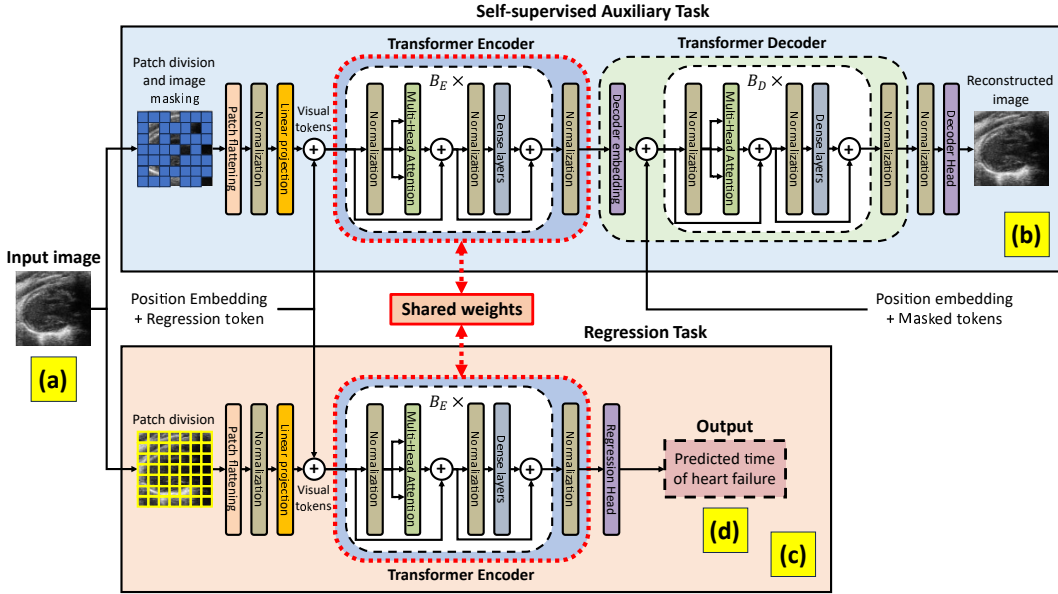


Figure 5: Architecture of the proposed deep neural network with the training approach based on self-supervised learning. (a) The input: an image from an echocardiography video sequence, in the form of an original echocardiography sample, a mode, or a reconstruction obtained with the SVD and the HODMD algorithms, result from the Modal Decomposition-based Data Transform phase. (b) The Self-supervised Auxiliary Task, aimed to reconstruct the missing patches from the masked image, aiding in training the ViT for the regression task. (c) The Regression Task, the one of interest, for heart failure time prediction. (d) The predicted heart failure time of the input image.

The backbone which processes the visual tokens is based on a Transformer Encoder, whose weights are shared with the Transformer Encoder used for the Self-supervised Auxiliary Task, learned at the same time (highlighted in red in Fig. 5). This has been done following the configuration of the ViT-T (Tiny) architecture, the shallowest one, to minimize overfitting (Das et al. (2024)), which is as follows: twelve stacked Transformer blocks (so $B_E = 12$). Each Transformer block includes a multi-head attention layer, with three heads, projection dimension 192, and without dropout.

An empty branch (skipped connection) and dense layers with two units follow the multi-head attention layer, each one composed of a fully connected layer with the Gaussian Error Linear Unit (GELU) activation function. The use of skip connections addresses the vanishing gradient problem, inherent to deep neural networks, to considerably improve training convergence. The ratio of the dense layers used is 4, that is, the number of hidden features is four times the amount of input features. The Transformer block finally introduces a skip connection, connecting the output of the previous one to the output of these dense layers. After all the B_E Transformer blocks, features are normalized and introduced into a regression head, whose output is the estimation of the time in which a heart failure will happen (Fig. 5 (d)), according to the input image (Fig. 5 (a)).

Regarding the Self-supervised Auxiliary Task (Fig. 5 (b)), the processing is based on the MAE (He et al. (2022)). That is, first, patches from the input image (Fig. 5 (a)) are randomly masked before the tokenization. After that, the same Transformer Encoder as the one for the Regression Task is used. Precisely, the weights between both Transformer Encoders are shared (highlighted in red in Fig. 5). Therefore, during training, these weights are adapted to both tasks, improving the discriminating capability of the ViT used for heart failure time prediction, even with scarce databases. After the B_E Transformer blocks, a Transformer Decoder is used for the reconstruction of the missing patches, much shallower than the Encoder. This Decoder has been designed by first incorporating a decoder embedding which adapts the projection dimension to 128 via a fully connected layer. After adding the masked tokens and the position embedding, two stacked Transformer blocks have been used ($B_D = 2$). Each of these blocks includes a multi-head attention layer with 16 heads. Similarly, empty branches and dense layers with two units and a ratio of 4, each one with the GELU activation function, have also been employed. After all the B_D Transformer blocks, features are normalized, the regression token is removed, and a decoder head is used for the reconstruction of the missing patches.

Considering the joint learning on both tasks at the same time, the final convex loss function is as follows:

$$L = (\alpha \times L_{reg}) + [(1 - \alpha) \times L_{SSAT}], \quad (3)$$

where L_{reg} is the regression loss between the estimated heart failure time and the real one; L_{SSAT} is the loss component between the original and re-

constructed image, computed only for the masked patches (He et al. (2022)), and α is the loss scaling factor, weighing the importance of each task. Both loss functions are based on the Mean Square Error (MSE). Note that, after training, like in the usual approach of MAEs (He et al. (2022)), for the Deep Neural Network-based Heart Failure Prediction phase, only the branch concerning the Regression Task (Fig. 5 (c)) is used, and the branch about the Self-supervised Auxiliary Task (Fig. 5 (d)) is discarded.

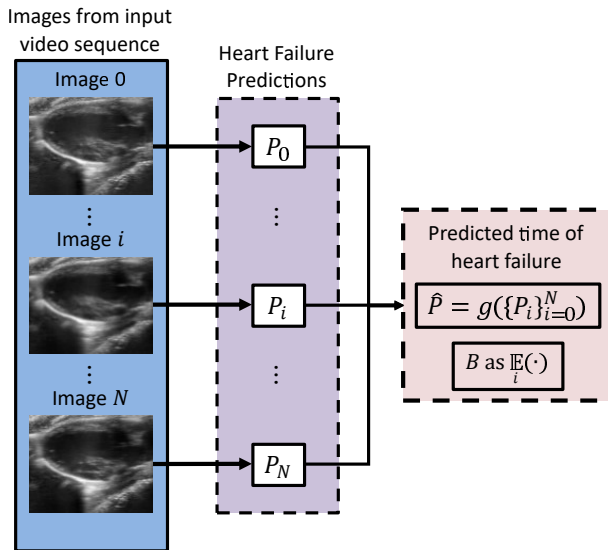


Figure 6: Illustration of the Fusion of Heart Failure Predictions phase. The predictions corresponding to the times of happening a heart failure are fused, and the average value determines the estimated time of the heart failure of a test sequence.

The deep neural network uses the annotated cardiac database of images, \mathbf{D}_{train} , obtained in the Cardiac Database Creation stage described in Subsection 2.1 for training. Concerning the optimization technique, the AdamW algorithm has been used. The employed learning rate strategy is based on the warm-up cosine policy (Lee et al. (2021)) that computes the learning rate at iteration i by the expression $\lambda_i = 0.5 \times \lambda_t \times (1 + \cos(\pi \times (i - N_w) / (N_{iter} - N_w)))$, where N_{iter} is the maximum number of iterations. Following the configurations used in Das et al. (2024), the target learning rate is fixed to $\lambda_t = 2.5e-4$, and the warmup steps N_w to 5. The momentum and weight decay are set to 0.9 and 0.05, respectively. The batch size has been set to 64 images due to the limitations of the physical memory of the GPUs available (Nvidia A100 and Nvidia RTX A4500). About the database division, a

splitting scheme of 60% – 20% for training and validation, respectively, has been adopted, balancing the cardiac categories to ensure that every set contains approximately the same number of samples for each heart state. The batch generation scheme includes data augmentation techniques based on geometric transformations (namely: resizing, random horizontal flips, and random erasing), applied to the echocardiography data. In this way, the model becomes more robust to different perspectives acquired of the heart. In addition, these data augmentation techniques complement to the Modal Decomposition-based Data Generation phase already explained in Subsection 2.1, marginally improving the performance compared to the modal decomposition.

In the fourth and last phase, Fusion of Heart Failure Predictions, an estimation of the time of happening a heart failure in the input test sequence is determined by combining multiple predictions. This process is illustrated in Fig. 6. Each image i from the $N + 1$ images depicted were obtained from the input test sequence according to the process explained in the second phase, Modal Decomposition-based Data Transform. That is, these images can be either original echocardiography images, or modes or reconstructions obtained with the SVD and HODMD modes. Then, each of these images is processed by the deep neural network as explained in the third phase, Deep Neural Network-based Heart Failure Prediction. Therefore, each of these images has associated a time prediction P_i , that is, the estimation of the age of the patient in which a heart failure will happen. The set of time predictions $\{P_i\}$ is then used to compute a unique time prediction associated to the input test sequence \hat{P} . For this purpose, the average has been used. As a result, an estimation of the time in which a heart failure will happen is obtained. Note that relying on a sequence of echocardiography images instead of a single image to predict the time of heart failures is more robust, as using more data can help doctors to make more confident heart prognoses. In addition, certain heart pathologies might lead to arrhythmias or patterns in the heart cycles which, therefore, constitute temporal information which can be obtained from sequences, and which could be valuable to accurately predict heart failures.

3. Database

The heart failure prediction system here proposed has been tested and validated using a database of echocardiography images. It is composed of video

sequences representing the following heart states: Control (CTL), Obesity (OB), and Systemic Hypertension (SH). This database has been elaborated in a collaboration with the Centro Nacional de Investigaciones Cardiovasculares (CNIC). A sample image from each of these heart states is shown in Fig. 7. As can be seen, echocardiography imaging inherently has much noise, as expected in this modality of data. In addition, different perspectives are taken, increasing the complexity of the heart failure prediction task. Only the area of the heart, i.e., the region of interest (ROI), is taken for the prediction system, as specified in the Data Homogenization phase described in Subsection 2.1. The obtained heart areas have different resolutions, showing the heterogeneity of the echocardiography imaging: in mean and standard deviation, the spatial resolution is $(675.68 \pm 47.28) \times (583.15 \pm 0.49)$ pixels. However, the aspect factor among the images barely changes and is close to 1, so these are practically square: 1.16 ± 0.08 . Therefore, resizing to square images for the deep neural networks barely deforms the heart areas, and does not suppose a degradation of the heart failure prediction performance, as preserving the spatial features characterizing the different heart states.

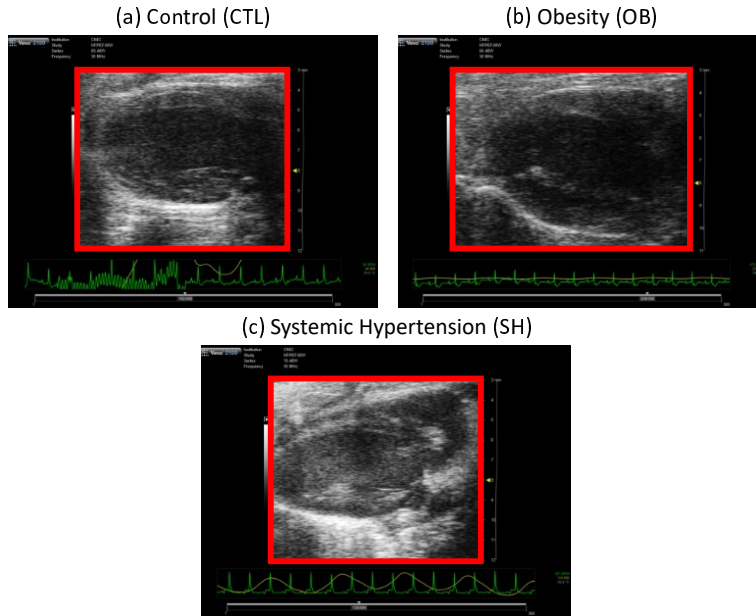


Figure 7: Sample images from the different heart states of the echocardiography data. The regions of interest are delimited by the red boundaries.

A summary of the main characteristics of the cardiac database is pre-

sented in Table 1. It includes information about the times in which heart failures happen. An average and a standard deviation of the age of the heart failure event are represented for each heart state. As can be seen, unhealthy classes (OB, and SH) tend to have earlier heart failures than in the case of healthy hearts (CTL), as expected. This cardiac database is composed of the original echocardiography images, and the associated SVD-based data and the HODMD-based data. These data have been generated according to the process made in the Modal Decomposition-based Data Generation phase described in Subsection 2.1. That is, the SVD-based data were obtained by applying the SVD algorithm on each video sequence of echocardiography images. For each of these sequences, reconstructions and modes were obtained with the SVD algorithm (denoted as \mathbf{D}_{SVD1-R} and \mathbf{D}_{SVD1-M} , respectively, following the notation from Subsection 2.1). After that, the HODMD-based data were generated by applying the HODMD algorithm on each sequence, but using their associated SVD reconstructions instead of the original images. As a result, for each sequence, reconstructions and modes were obtained ($\mathbf{D}_{HODMD-R}$, $\mathbf{D}_{HODMD-M}$, respectively). Finally, the SVD algorithm was applied on each sequence, using their associated HODMD modes, taking in this case the reconstructions (\mathbf{D}_{SVD2-R}). In Table 1, the column ‘# Snapshots’ indicates the total number of original snapshots of the sequences. Note that this number equals the number of associated reconstructed ones after applying the SVD algorithm, and also the number of reconstructions obtained after using the HODMD algorithm. The columns ‘# SVD modes’ and ‘# HODMD modes’ represent the total number of SVD modes and of HODMD modes obtained, respectively. The aim of generating the SVD-based data and the HODMD-based data is to address the difficulty in the medicine field to elaborate a varied database with high quality enough to properly train deep learning algorithms, as implying high costs and very hard specialized work. Also note that the training, validation and test sets comprise different sequences, which are the ones that both achieve the splitting scheme proposed in this work and a reasonable balance in the number of samples in each class.

Table 2 shows the experimented cases of the training database \mathbf{D}_{train} , each one indicating which types of data are used to form that. Different types of test data, resulting from the Modal Decomposition-based Data Transform phase described in Subsection 2.2, have also been assessed. In this way, the impact of each type of data on the final performance could be evaluated, including the robustness to noise, as the original echocardiography imaging

Table 1: Summary of the main characteristics of the cardiac database.

Heart State	Age of heart failure (months)	Set	# Sequences	# Snapshots	# SVD Modes	# HODMD Modes
Control (CTL)	23.86 ± 5.23	Training	35	10 204	175	1334
		Validation	12	3496	60	457
		Test	9	2619	45	321
Obesity (OB)	22.03 ± 6.35	Training	28	8170	140	1140
		Validation	9	2700	45	369
		Test	11	3194	55	412
Systemic Hypertension (SH)	20.77 ± 6.65	Training	31	8919	155	1186
		Validation	12	3136	60	422
		Test	10	3000	50	380
Total			157	45 438	785	6021

Table 2: Summary of the combinations for \mathbf{D}_{train} used in the Cardiac Database Creation stage.

Case	SVD-based Data			HODMD-based Data		SVD (DMD Modes)	# Training Samples
	\mathbf{D}_{orig}	\mathbf{D}_{SVD1_R}	\mathbf{D}_{SVD1_M}	\mathbf{D}_{HODMD_R}	\mathbf{D}_{HODMD_M}	\mathbf{D}_{SVD2_R}	
1	×						27 293
2		×					27 293
3	×	×	×				55 056
4	×	×					54 586
5		×	×				27 763
6				×			27 293
7				×	×		38 273
8		×		×			54 586
9	×	×		×			81 879
10				×	×	×	49 253
11		×	×	×	×		66 036
12		×	×	×	×	×	77 016
13	×	×	×	×	×		93 329
14	×	×	×	×	×	×	104 309

inherently has much noise. Note that the absolute value, the real, and the imaginary parts of the HODMD modes have been taken to increase the number of samples (i.e., images) of the database and so to obtain the total number of training samples in each case. Also note that the final column, i.e., SVD (HODMD Modes), represents the use of the reconstructions of the HODMD modes after applying the SVD algorithm on them, that is, \mathbf{D}_{SVD2_R} , according to the notation presented in Subsection 2.1. Similarly, the absolute value, and the real and imaginary parts have been taken to increase the database.

4. Results

The algorithm considered in this paper has been tested with the cardiac database using the different cases for the training database \mathbf{D}_{train} presented in Table 2. Additionally, it has been compared with ViT and CNN-based algorithms, including DeiT (Touvron et al. (2021)), ResNet50-version 2 (He et al. (2016)), and Swin-version 2 (Liu et al. (2022)).

The following metrics have been utilized to measure the performance of each algorithm in terms of heart failure prediction accuracy and computational cost: mean (μ) and standard deviation (σ) of the predicted age of heart failure, estimation error, the root mean squared error (*RMSE*, or error margin), maximum and minimum errors, estimated floating point operations per second (GFLOPs, or Gigaflops), and average processing time per image \bar{t} .

The mean (μ) and standard deviation (σ) of the predicted age of heart failure are calculated for each heart state using the computed values of heart failure times of all the corresponding test video sequences. That is, given a set of predicted times of heart failures corresponding to the test video sequences of a determined heart state y , $\{\hat{P}_j\}$, the mean and the standard deviations for this heart state are calculated based on the set as follows:

$$\begin{aligned}\mu &= \mathbb{E}[\{\hat{P}_j\}]. \\ \sigma &= \sqrt{\mathbb{E}[(\{\hat{P}_j\} - \mu)^2]}.\end{aligned}\tag{4}$$

The estimation error in a test sequence j is the difference between the associated predicted time of heart failure \hat{P}_j and the true time T_j , expressed as $\hat{P}_j - T_j$. Derived from this, the root mean squared error (*RMSE*, or error margin from now on), and the maximum and minimum errors are computed for each heart state as follows:

$$\begin{aligned}RMSE &= \sqrt{\mathbb{E}[(\{\hat{P}_j\} - \{T_j\})^2]}. \\ Max\ error &= \max(\{\{\hat{P}_j\} - \{T_j\}\}). \\ Min\ error &= \min(\{\{\hat{P}_j\} - \{T_j\}\}).\end{aligned}\tag{5}$$

The maximum and minimum errors have been represented with and without sign (that is, in absolute value). For brevity, error with sign is denoted

as (w/), and error without sign as (w/o). Therefore, in the case of errors represented with sign, if $\hat{P}_j - T_j < 0$, the predicted time would indicate that the heart failure would happen sooner than the real time of heart failure, and it would be later otherwise. Unless the contrary is explicitly indicated, the heart failure times are represented in months.

The average processing time per sample \bar{t} is the average time taken by the proposed system to process a sample (either image or sequence) and give the heart failure prediction. It is broken down into the SVD algorithm (\bar{t}_{SVD}), the HODMD algorithm, comprising the HOSVD dimensionality reduction (\bar{t}_{HOSVD}) prior to the HODMD itself (\bar{t}_{HODMD}) (Bell-Navas et al. (2023)), and the Deep Neural Network-based Heart Failure Prediction phase (\bar{t}_{pred}). The throughput is measured in frames per second, fps, and represents the number of snapshots which can be processed by the deep neural network in a second. Therefore, this metric assesses the capability of the deep neural network for real-time applications. The throughput is calculated as $1/\bar{t}_{pred}$. Unless the contrary is explicitly specified, the times representing computational cost are measured in milliseconds.

The results have been obtained using a cluster with Intel Xeon Gold 6240R, AMD Ryzen Threadripper PRO 5995WX, three Tesla A100 GPU, and four Nvidia RTX A4500 working in parallel for training, and Intel Xeon Gold 6230 and one Tesla V100 GPU for testing. In this way, not only the high amount of data conforming the created cardiac database is managed, but also the training convergence is speeded up and eased.

4.1. Performance evaluation using different types of data

First, the performance in terms of heart failure prediction accuracy on the training cases and on different types of data used for test, i.e., test data obtained with the Modal Decomposition-based Data Transform phase described in Subsection 2.2, is presented. To that end, the configuration of the SVD and HODMD algorithms, the deep neural network, and of the prediction is initially introduced. Later on, the influence of the types of data used for both training and test on the overall performance of the system is studied. Lastly, the heart failure prediction performance in each heart state for the best configuration is shown.

1. Configuration: The configuration for the Modal Decomposition-based Data Generation and Transform phases is as follows. For the SVD algorithm, the number of modes provided has been set to 5, considered

adequate for fair reconstructions with the noise filtered according to the contribution of the modes in the frames. Regarding the HODMD algorithm, the minimum number of snapshots a sequence must have to be able to apply the HODMD algorithm has been set to 100, following the practices of Groun et al. (2022). In this way, at least three heart cycles are covered, considered enough to obtain fair reconstructions and to correctly characterize the temporal information. Moreover, the number of snapshots taken from each sequence K has been set to the total number of frames of the corresponding sequence. In this way, the maximum number of cardiac cycles possible can be captured and the cardiac and respiratory frequencies can be more accurately obtained, and so modes characterizing the physics of the data. The time interval between snapshots $\Delta t = 4 \text{ ms}$ and the tolerances $\epsilon_{SVD} = \epsilon_{DMD} = 5e-4$ have been selected according to Groun et al. (2022): on the one hand, the value of Δt is based on the used ultrasound scanner, configured by a specialist, in the way that the images acquired properly give the cardiac and respiratory frequencies. On the other hand, regarding the selected tolerances for the dimensionality reduction and amplitude truncation steps, respectively, these are larger than the noise level, and lead to a reasonable number of frequencies and so characteristic modes associated with the studied heart states and the heart failures. The index d has been configured for each sequence in the way that fair reconstructions of the snapshots are obtained. In particular, $d = \lfloor K/5 \rfloor$ results adequate for these reconstructions. Precisely, this value of d follows the recommendations for the calibration process described in Le Clainche and Vega (2017). In fact, other values of d lead to reconstructions with severe distortions and artifacts which do not describe the dynamics of the data and do not adequately reproduce the heart cycles. Therefore, discriminative features associated with the heart states and leading to more accurate heart failure predictions are not extracted in these cases.

Concerning the Deep Neural Network-based Heart Failure Prediction phase, the input images have been resized to 224×224 , and the patch size has been set to 16. For the self-supervised learning, patches are masked randomly with a ratio of 0.75. This is due to the memory limitations of the GPU devices available, while giving a high amount of patches for a more proper training. In addition, as already specified in Subsection 2.2, according to the configuration of the Transformer Encoder, the ViT architecture used corresponds to ViT-T (Tiny) (Das et al.

(2024)), which leads to the shallowest neural network architectures. Precisely, other configurations leading to deeper models have not been tried for this reason. In addition, deeper models would be too complex and more prone to overfitting in the actual scenario of scarce number of samples, worsening the performance. On the other hand, the adoption of the decoder configuration follows the usual parameters from He et al. (2022) for the MAE. On the other hand, the scaling factor used to weight the training loss components is $\alpha = 0.1$, according to Das et al. (2024). Therefore, obtaining an effective representation learning of the echocardiography images is emphasized (see Eq. 3 in Subsection 2.2).

Finally, regarding the Fusion of Heart Failure Predictions phase, the average of the predicted time values of happening a heart failure has been used to calculate the global predicted time for the test sequence.

Table 3: Error margin results comparing different types of data for test and training cases using the proposed framework (best results in **bold**, in Case 14). Refer to Table 2 for the specifications of each training case.

		Error margin													
		Case 1	Case 2	Case 3	Case 4	Case 5	Case 6	Case 7	Case 8	Case 9	Case 10	Case 11	Case 12	Case 13	Case 14
SVD	Original	4.75	5.05	4.67	5.12	4.58	5.53	4.57	5.55	4.78	4.65	4.59	4.63	4.56	4.54
	Reconstructions	5.09	5.30	4.70	5.19	4.59	5.80	4.57	5.62	4.90	4.65	4.60	4.64	4.56	4.55
	Modes	7.08	7.23	4.72	5.58	4.75	6.73	4.71	7.29	6.71	4.70	4.69	4.72	4.66	4.61
HODMD	Reconstructions	5.10	5.23	4.69	5.18	4.59	5.78	4.57	5.60	4.89	4.65	4.60	4.64	4.56	4.55
	Modes (abs)	4.87	4.55	6.01	4.72	4.67	4.80	4.84	5.05	5.33	4.59	4.75	4.65	4.71	4.53
# Samples (train)		27 293	27 293	55 056	54 586	27 763	27 293	38 273	54 586	81 879	49 253	66 036	77 016	93 329	104 309

- Performance: Table 3 reveals the impact of using the different types of data for testing and of the training cases presented in Table 2 on the heart failure time prediction performance of the proposed system. In this table, the error margin has been represented. The training cases lead to a general improvement, because of the decreasing error margin values, with respect to the case 1 (with only original images), considering that, in general, more training samples are available, as expected. Precisely, the case 14 which considers all types of data (original images and both SVD and HODMD modes and reconstructions) leads to the best error margin: 4.54 months. On the other hand, in this case 14, the performance barely changes, regardless of the type of testing data used, which demonstrates the robustness of the proposed system to noise and to different types of data. On the other hand, the training cases affect the variation of the performance: for example, the case 9, which has more samples than the case 11, leads to a

lower performance. The case 9 uses original images and reconstructions from both the SVD and the HODMD algorithms, but the other one, the case 11, incorporates modes instead of the original images. Also note that there is a consistent improvement in the training cases which incorporate HODMD modes, and also in those training cases which include the SVD reconstructions of the HODMD modes, which are the cases 7, 10, 11, 12, 13, and 14. Therefore, these two facts reveal the importance of using HODMD modes. This is due to that the HODMD modes describe the dynamics of the data and contain the temporal information useful for the ViT to distinguish the different heart states and so to determine a more accurate heart failure time. In addition, the data generated with the SVD and the HODMD algorithms have less noise than the original data (inherently with much noise), once more, leading to more discriminative features. This shows the importance of using the SVD and the HODMD algorithms for both data augmentation and extraction of more discriminative features associated to the different heart states, allowing more accurate heart failure prediction times. Therefore, these algorithms improve the discriminating capability of the proposed ViT in the usual scenario of having a scarce number of samples. In addition, this also demonstrates the usefulness of the modal decomposition techniques to deal with the difficulty to elaborate varied databases with high quality enough in the medical field in both costs and very hard specialized work. On the other hand, the results show the effectiveness of the SVD and of the HODMD algorithms to deal with the high amount of noise inherent to the original echocardiography images, leading to performance improvements, and making the proposed system more robust to noise. If another type of noise were added to the echocardiography images, the SVD and the HODMD algorithms would also effectively clean the data and would generate more discriminative features which lead to more accurate heart failure time predictions.

Table 4 presents the heart failure prediction results for each heart state using the best configuration inferred from Table 3: training case 14 and original images as test data. This kind of test data has been selected because of having more original images than modes, leading to more reliable prediction results in the fusion of the estimated heart failure times. The performance is balanced among the considered heart states, like the number of test samples in terms of both images and

sequences. A general error margin of 4.54 months is reached, which is accurate enough for medical applications considering the low number of original training samples (images) for each class, much lower than the samples required by typical deep learning algorithms (hundreds of thousands or even millions of samples). This means that, if a much higher number of samples were available, the heart failure times would be more accurately predicted and the features associated to the different heart states better learned. However, this is unfeasible, considering the high difficulty in terms of costs and specialized hard work in the medical field. On the other hand, the means (μ) and standard deviations (σ) of the real and predicted ages of heart failures are similar, which means that the proposed system can follow the statistics of the real ages of heart failures under the different heart states, and therefore estimate heart failure times close to the real ones. Therefore, the results obtained demonstrate the capability of the proposed ViT to effectively model the non-linear relationship which could be present between the input and the output: in this case, between echocardiography images and heart failure times.

4.2. Comparison with Alternative Algorithms

In this second part of the experiments, the performance of the proposed system has been compared against other alternative deep neural networks. This is, using the same framework, the proposed ViT has been replaced by other deep neural networks. In particular, the compared deep neural networks are DeiT (Touvron et al. (2021)), ResNet50-version 2 (He et al. (2016)), and Swin-version 2 (Liu et al. (2022)). These deep neural networks have been selected for the comparisons to cover a range of competitive CNNs and ViTs which introduce alternative mechanisms for better training regarding the architecture and adoption of auxiliary databases. First, the configuration of the proposed system is introduced. Next, the configuration and the necessary adaptations of the alternative algorithms are described. Finally, an overall performance comparison between the proposed ViT and the other deep neural networks is presented, using the most representative training cases (1, 7, 10, 11, 12, 13, 14) and the main types of test data (Original, HODMD-based reconstructions, and HODMD modes).

1. Configuration and adaptation of the alternative algorithms: The configuration of the SVD and HODMD algorithms, the ViT, and of the prediction, is the same as already described in Subsection 4.1.

Table 4: Heart failure time prediction performance for the studied heart states using μ , σ , error margin, maximum and minimum errors (with: w/, and without sign: w/o) obtained with the best configuration of the proposed framework (training case 14 and original images as test data. Refer to Table 2 for the specifications of each training case).

Heart State	Age of heart failure ($\mu \pm \sigma$)			<i>Max error</i> (w/)	<i>Min error</i>			# Test samples	
	Real	Predicted	Error margin		(w/)	(w/o)	Images	Sequences	
Control (CTL)	27.83 \pm 0.00	23.52 \pm 0.91	4.41	- 2.81	- 6.29	2.81	2619	9	
Obesity (OB)	23.50 \pm 4.20	23.79 \pm 0.96	4.40	6.95	- 4.59	1.48	3194	11	
Systemic Hypertension (SH)	19.55 \pm 3.38	22.80 \pm 1.26	4.81	9.62	- 1.55	0.52	3000	10	
Total	23.48 \pm 4.59	23.38 \pm 1.14	4.54	9.62	- 6.29	0.52	8813	30	

Before introducing the configurations and parameters selected for the DeiT, ResNet50-v2, and Swin-v2, some considerations must be taken into account. Specifically, the input of these deep neural networks has three channels, but the cardiac database used in this work comprises one-channel data. In addition, their architectures were designed for classification into several classes, for example, for the ImageNet challenge classes (Russakovsky et al. (2015)). Therefore, adaptations were required to enable them to not only work with one-channel data, but also to perform regression, in this case, to predict heart failure times. To obtain three-channel data from the cardiac database, the input has been replicated three times and concatenated in the channel dimension before being introduced into the deep neural networks. For regression, the final layer of these models is replaced by a linear layer whose output is a single value, corresponding to the estimated time of happening a heart failure. For the initialization of ResNet50-v2, random weights have been tested, and also pretrained ones from the ImageNet challenge (Russakovsky et al. (2015)). This supposes a good initialization, and therefore improves the training convergence and the quality of the models obtained after fine-tuning using the cardiac database. This means that ResNet50-v2 uses an auxiliary dataset in addition to the cardiac database. As the proposed ViT and the rest of algorithms do not use that auxiliary dataset, this supposes an advantage for the algorithm. In addition, the compared algorithms, unlike the proposed ViT trained with the self-supervised learning approach, use mixup in addition to the conventional data augmentation techniques and the modal decomposition to augment the databases. This is because the use of mixup worsens the performance of the proposed ViT with self-supervised learning, but improves the performance in the rest of algorithms. This could be

because mixup hampers the feature representation learning made by the MAE.

Similarly to the proposed ViT, the input images have been resized to 224×224 . However, in the Swin-v2, the input image size has been set to 256×256 . This image resizing is also mandatory because of the memory limitations of the GPU devices for training. The patch size in the DeiT is also 16, and the window size in the Swin-version 2 is 16 pixels as well. The tested DeiT and Swin-v2 architectures are DeiT-S and Swin-v2-T, respectively (i.e., Small and Tiny). In addition, the Local InFormation Enhancer (LIFE) (Akkaya et al. (2024)) module has been included in the DeiT-S and Swin-v2-T architectures to increase the receptive fields of the embeddings in their self-attention blocks by including patch-level local information. In this way, the proposed self-supervised approach is compared against the LIFE module as methods to increase the locality inductive bias in ViTs.

2. Performance: Table 5 presents a comparison of the heart failure time prediction performance in terms of the error margin, using the cardiac database and the proposed system with either the ViT trained with the proposed self-supervised learning approach, DeiT-S, Swin-v2-T, or ResNet50-v2, with pretraining or with no pretraining. Only the training cases 1, 7, 10, 11, 12, 13, and 14 from Table 2 have been considered, as being the most representative ones regarding the contribution of the SVD and HODMD algorithms with respect to the use of only original images. Regarding the types of test data, original images, HODMD-based reconstructions and HODMD modes have been compared, as mainly representing the influence of the SVD and HODMD algorithms as feature extractors.

As can be observed in the table, the two best results in terms of heart failure prediction performance have been obtained using the proposed ViT and the Swin-v2-T, according to the error margins represented. Moreover, these algorithms even outperform ResNet50-v2, showing the efficacy of using more complex models, consisting in Transformers which incorporate mechanisms to better train them and adapt them more to scarce datasets (e.g., the LIFE module to increase the receptive field in the inputs of the attention mechanisms in the case of the Swin Transformer, or the self-supervised learning approach proposed for the ViT). As deep neural networks, both show that they can effectively model the non-linear relationships which could be present be-

tween echocardiography imaging and heart failure times. On the other hand, there is a general improvement in the training cases with respect to the case 1 and when using the HODMD modes for test data instead of original images. Therefore, the alternative algorithms can also benefit from the use of the SVD and HODMD algorithms for both data augmentation and feature extraction, also incorporating temporal information thanks to the HODMD modes. Once more, this improvement also demonstrates the effectiveness to address the high noise inherent to the original echocardiography images and, therefore, the robustness of the proposed system with the alternative algorithms to noise. Again, other kinds of noise additionally added to the echocardiography imaging would be effectively reduced by the SVD and HODMD algorithms, leading to performance improvements with the alternative algorithms. On the other hand, note that, in the training cases without SVD nor HODMD modes, like the case 1, a better performance is generally achieved when using original test images instead of modes. This can be attributed to the fact that the models learn to predict heart failures in original images, obtaining more confident predictions in the original images than in other representations.

Overall, the proposed ViT with the self-supervised learning approach achieves the best results. However, the Swin-v2-T performs very closely to it. This is mainly because the Swin-v2-T used incorporates the LIFE module (Akkaya et al. (2024)), the augmentation based on mixup (which worsens the performance in the case of the proposed ViT with self-supervised learning) and shifted windows to increase local self-attention. All of this reduces the dependence on very large databases for a proper training. Even with the mechanisms, a larger cardiac database could significantly improve the proposed framework with the alternative models, trained from scratch or not. On the other hand, according to the results with ResNet50-v2, the adoption of natural images for transfer learning would not suppose an effective alternative to the cardiac database for the performance improvement. This is because medical images, like echocardiograms, have different characteristics to those of natural images like in the ImageNet database. Specifically, echocardiography images are based on standardized views, in this case more focused on the region of the heart, and features with subtle fine texture differences, also with usually different pixel intensity distributions due to the different acquisition conditions. On the contrary,

natural images focus on broader, more easily distinguishable patterns, and contain high-level semantic features which could not be useful for medical imaging tasks like heart disease recognition or heart failure prediction, explaining poor performances of pretrained models like in Farhad et al. (2023).

Regarding the results obtained, the training cases with HODMD-based data have led to the best performances among the compared algorithms. In the specific case of the proposed ViT, the training case 14 gives the best results (error margin of 4.54 months), showing the contribution of all types of data. In general, the use of original images or SVD-based data for training can also increase the final performance, although with a lower difference, as can be seen in the case of Swin-v2-T.

Table 6 summarizes the computational cost of the different phases of the prediction process. Note that the time measures represented in the table are averages per image, although the SVD and the HODMD algorithms are applied on sequences rather than on single images. As can be seen, the HOSVD dimensionality reduction process implies the highest computational cost by far (Bell-Navas et al. (2023)). On the other hand, the proposed ViT trained with self-supervised learning is practically the fastest deep learning algorithm, with a much higher throughput than the one of Swin-v2-T, which is desirable for several real-time medical applications. The proposed ViT has a similar \bar{t}_{pred} than the one obtained with ResNet50-v2, but the proposed ViT achieves a better trade-off between computational cost and prediction performance. In addition, the proposed ViT has the lowest number of learnable parameters among the compared algorithms. Therefore, these results encourage the deployment of the proposed ViT using less resources. In every case, all time values are inside of real-time requirements, which is appealing for several applications in the medical field, for example, in portable devices, allowing to cover more remote areas.

In summary, the proposed ViT achieves the best overall performance in terms of both heart failure prediction and operation time. This is achieved using only the proposed self-supervised learning approach, and so with no other external databases, unlike ResNet50-v2. This supposes an advantage, because of reducing training computational resources, and the dependence on very large training datasets with high quality. Lastly, heart failure prediction is expected to be more accurate with larger medical image databases based on heart diseases

with annotations of the times of heart failures.

Table 5: Comparison of the heart failure time prediction performance in terms of the error margin among different deep neural networks using the main types of test data and the main training cases (best results in **bold**, in Case 14). Refer to Table 2 for the specifications of each training case.

		Error margin						
Algorithm	Test Data	Case 1	Case 7	Case 10	Case 11	Case 12	Case 13	Case 14
DeiT-S	Original	4.81	4.58	4.64	4.89	5.09	4.84	5.43
	HODMD Reconstructions	4.87	4.58	4.66	4.88	5.19	4.93	5.46
	HODMD Modes	4.73	4.60	4.64	4.90	4.85	4.76	5.28
Swin-v2-T	Original	5.07	4.61	4.62	4.54	4.79	4.93	4.54
	HODMD Reconstructions	5.09	4.61	4.62	4.55	4.83	4.97	4.54
	HODMD Modes	7.91	4.64	4.60	4.60	4.60	4.82	4.62
ResNet50-v2	Original	5.21	4.77	4.74	4.78	4.87	4.86	5.04
	HODMD Reconstructions	4.87	4.77	4.93	4.95	4.94	4.94	5.06
	HODMD Modes	4.98	4.86	4.74	4.74	4.83	5.01	4.86
ResNet50-v2-pretrained	Original	5.20	5.50	4.81	4.81	4.56	4.93	5.01
	HODMD Reconstructions	4.87	4.80	4.71	4.90	4.91	4.83	4.96
	HODMD Modes	7.06	4.79	4.73	4.81	4.77	4.72	4.83
Proposed	Original	4.75	4.57	4.65	4.59	4.63	4.56	4.54
	HODMD Reconstructions	5.10	4.57	4.65	4.60	4.64	4.56	4.55
	HODMD Modes	4.87	4.84	4.59	4.75	4.65	4.71	4.53
# Samples (train)		27 293	38 273	49 253	66 036	77 016	93 329	104 309

Table 6: Computational cost of different phases of the heart failure time prediction system using the algorithms compared.

Model	# Parameters (M)	GFLOPs	\bar{t}_{SVD}	\bar{t}_{HOSVD}	\bar{t}_{HODMD}	\bar{t}_{pred}	Throughput
DeiT-S	21.81	4.64				27.05	36.98
Swin-v2-T	27.73	6.75	5.1	591	0.648	18.96	52.84
ResNet50-v2	23.51	4.11				7.44	134.82
Proposed	6.01	1.68				9.71	105.76

5. Conclusions

Heart diseases are the main cause of human mortality in the world. Thus, the early identification of heart diseases is a task of great importance. In this work, a real-time heart failure prediction system for echocardiography video sequences has been presented to specifically address this challenging and demanding task, which has not been addressed in the related literature to the best of the authors’ knowledge. The two major contributions of this paper

are the creation of a large annotated cardiac database from echocardiography sequences with heterogeneous acquisition features; and a deep neural network, based on a ViT, trained using a self-supervised learning approach which effectively improves the performance with scarce datasets. These two contributions, acting synergistically, successfully address the usual challenge of having a scarce number of samples in the medicine field, reducing the dependence on very large training datasets. More precisely, the elaboration of varied databases with high quality enough is very difficult, implying high costs and very hard specialized work from experts in heart diseases. In addition, the general trend in the related literature about heart disease recognition and heart failure prediction in echocardiography images barely explores self-supervised learning, even less Masked Autoencoders (MAE), to deal with this typical situation of scarce databases. This implies the necessity to adopt techniques specifically designed to address this problem. In the creation process of the database, the HODMD algorithm has been employed as a feature extractor and as a data augmentation technique. This algorithm has demonstrated to improve the heart failure time prediction performance, as also incorporating temporal information from the HODMD modes, useful to better characterize the different heart states and so to more accurately estimate the times of heart failures. The results obtained have proved that the proposed system performs better than ResNet-v2 (even with pretraining), and also better than other ViTs, which incorporate additional local information of patches with the LIFE module. We conclude that, if longer image datasets, and also from other modalities, about heart failures were available, overfitting would be reduced and robustness would be enhanced.

Declaration of competing interest

The authors declare the following financial interests/personal relationships which may be considered as potential competing interests: Andrés Bell-Navas reports financial support was provided by Spanish Ministry of Science and Innovation. Enrique Lara-Pezzi reports financial support was provided by Spanish Ministry of Science and Innovation. Soledad Le Clainche reports financial support was provided by the Ministerio de Ciencia, Innovación y Universidades. Enrique Lara-Pezzi reports financial support was provided by Comunidad de Madrid. María Villalba-Orero reports financial support was provided by Comunidad de Madrid. María Villalba-Orero reports financial support was provided by Juan de la Cierva Incorporación. Enrique Lara-

Pezzi reports a relationship with Spanish National Cardiovascular Research Center that includes: employment and funding grants. María Villalba-Orero reports a relationship with Spanish National Cardiovascular Research Center that includes: employment and funding grants. If there are other authors, they declare that they have no known competing financial interests or personal relationships that could have appeared to influence the work reported in this paper.

Acknowledgements

The authors acknowledge the Grants TED2021-129774B-C21, TED2021-129774B-C22 and PLEC2022-009235, funded by MCIN/AEI/10.13039/501100011033 and by the European Union "NextGenerationEU"/PRTR, and the Grant PID2023-147790OB-I00, funded by MICIU/AEI/10.13039/501100011033/FEDER, UE: the first one to A.B-N, the next two to E.L-P, and the last one to S.L. The authors also acknowledge the Grant PEJ-2019-TL/BMD-12831 from Comunidad de Madrid to E.L-P and to M.V-O, and a Juan de la Cierva Incorporación Grant (IJCI-2016-27698) to M.V-O. The CNIC is supported by the Instituto de Salud Carlos III (ISCIII), the Ministerio de Ciencia, Innovación y Universidades (MICIU), and the Pro CNIC Foundation, and is a Severo Ochoa Center of Excellence (Grant CEX2020-001041-S funded by MICIU/AEI/10.13039/501100011033).

Data availability

The data that have been used are confidential. For further details, please contact with Enrique Lara-Pezzi (elara@cnic.es).

References

- Akerman, A.P., Porumb, M., Scott, C.G., Beqiri, A., Chartsias, A., Ryu, A.J., Hawkes, W., Huntley, G.D., Arystan, A.Z., Kane, G.C., et al., 2023. Automated echocardiographic detection of heart failure with preserved ejection fraction using artificial intelligence. *JACC Adv.* 2, 100452.
- Akkaya, I.B., Kathiresan, S.S., Arani, E., Zonooz, B., 2024. Enhancing performance of vision transformers on small datasets through local inductive bias incorporation. *Pattern Recognit.* 153, 110510.

- Arooj, S., Rehman, S.u., Imran, A., Almuhaimeed, A., Alzahrani, A.K., Alzahrani, A., 2022. A deep convolutional neural network for the early detection of heart disease. *Biomedicines* 10, 2796. doi:<https://doi.org/10.3390/biomedicines10112796>.
- Behnami, D., Luong, C., Vaseli, H., Abdi, A., Girgis, H., Hawley, D., Rohling, R., Gin, K., Abolmaesumi, P., Tsang, T., 2018. Automatic detection of patients with a high risk of systolic cardiac failure in echocardiography, in: *Int. Workshop Deep Learn. Med. Image Anal.*, Springer. pp. 65–73.
- Bell-Navas, A., Groun, N., Garicano-Mena, J., Le Clainche, S., 2023. Optimized higher order dynamic mode decomposition analysis of electrocardiography datasets, in: *25th Conf. of ILAS*, pp. 91–92.
- Bell-Navas, A., Groun, N., Villalba-Orero, M., Lara-Pezzi, E., Garicano-Mena, J., Le Clainche, S., 2024. Automatic heart disease prediction using modal decomposition and masked autoencoders for limited echocardiography databases. *Int. J. Artif. Organs* 47, 471–472. doi:<https://doi.org/10.1177/03913988241279540>.
- Das, S., Jain, T., Reilly, D., Balaji, P., Karmakar, S., Marjit, S., Li, X., Das, A., Ryoo, M.S., 2024. Limited data, unlimited potential: A study on vits augmented by masked autoencoders, in: *Proc. IEEE Winter Conf. Appl. Comput. Vis.*, pp. 6878–6888.
- Farhad, M., Masud, M.M., Beg, A., Ahmad, A., Ahmed, L.A., Memon, S., 2023. A data-efficient zero-shot and few-shot Siamese approach for automated diagnosis of left ventricular hypertrophy. *Comput. Biol. Med.* 163, 107129. doi:<https://doi.org/10.1016/j.compbiomed.2023.107129>.
- Fazry, L., Haryono, A., Nissa, N.K., Hirzi, N.M., Rachmadi, M.F., Jatmiko, W., et al., 2022. Hierarchical vision transformers for cardiac ejection fraction estimation, in: *2022 7th Int. Workshop Big Data Inf. Secur. (IWBIS)*, IEEE. pp. 39–44.
- Groun, N., Villalba-Orero, M., Casado-Martín, L., Lara-Pezzi, E., Valero, E., Le Clainche, S., Garicano-Mena, J., 2025. Eigenhearts: Cardiac diseases classification using eigenfaces approach. *Comput. Biol. Med.* 192, 110167. doi:<https://doi.org/10.1016/j.compbiomed.2025.110167>.

- Groun, N., Villalba-Orero, M., Lara-Pezzi, E., Valero, E., Garicano-Mena, J., Le Clainche, S., 2022. Higher order dynamic mode decomposition: From fluid dynamics to heart disease analysis. *Comput. Biol. Med.* 144, 105384. doi:<https://doi.org/10.1016/j.compbiomed.2022.105384>.
- He, K., Chen, X., Xie, S., Li, Y., Dollár, P., Girshick, R., 2022. Masked autoencoders are scalable vision learners, in: *Proc. IEEE Comput. Soc. Conf. Comput. Vis. Pattern Recognit.*, pp. 16000–16009.
- He, K., Zhang, X., Ren, S., Sun, J., 2016. Identity mappings in deep residual networks, in: *Comput. Vis. ECCV 2016: 14th European Conference, Amsterdam, The Netherlands, October 11–14, 2016, Proceedings, Part IV 14*, Springer. pp. 630–645. doi:https://doi.org/10.1007/978-3-319-46493-0_38.
- Hetherington, A., Corrochano, A., Abadía-Heredia, R., Lazpita, E., Muñoz, E., Díaz, P., Maiora, E., López-Martín, M., Le Clainche, S., 2024. Modelflows-app: Data-driven post-processing and reduced order modelling tools. *Comput. Phys. Commun.* 301, 109217. doi:<https://doi.org/10.1016/j.cpc.2024.109217>.
- Le Clainche, S., Vega, J.M., 2017. Higher order dynamic mode decomposition. *SIAM J. Appl. Dyn.* 16, 882–925.
- Le Clainche, S., Vega, J.M., Soria, J., 2017. Higher order dynamic mode decomposition of noisy experimental data: The flow structure of a zero-net-mass-flux jet. *Exp. Therm. Fluid Sci.* 88, 336–353. URL: <https://www.sciencedirect.com/science/article/pii/S089417771730184X>, doi:<https://doi.org/10.1016/j.expthermflusci.2017.06.011>.
- Lee, S.H., Lee, S., Song, B.C., 2021. Vision transformer for small-size datasets. *arXiv preprint arXiv:2112.13492* .
- Liu, Z., Hu, H., Lin, Y., Yao, Z., Xie, Z., Wei, Y., Ning, J., Cao, Y., Zhang, Z., Dong, L., et al., 2022. Swin transformer v2: Scaling up capacity and resolution, in: *Proc. IEEE Comput. Soc. Conf. Comput. Vis. Pattern Recognit.*, pp. 12009–12019.
- Liu, Z., Huang, Y., Li, H., Li, W., Zhang, F., Ouyang, W., Wang, S., Luo, Z., Wang, J., Chen, Y., et al., 2023. A generalized deep learning model

- for heart failure diagnosis using dynamic and static ultrasound. *J. Transl. Intern. Med.* 11, 138–144.
- Muhtaseb, R., Yaqub, M., 2022. Echocotr: Estimation of the left ventricular ejection fraction from spatiotemporal echocardiography, in: *Med. Image Comput. Comput. Assist. Interv.*, Springer. pp. 370–379.
- Petmezas, G., Papageorgiou, V.E., Vassilikos, V., Pagourelas, E., Tsaklidis, G., Katsaggelos, A.K., Maglaveras, N., 2024. Recent advancements and applications of deep learning in heart failure: A systematic review. *Comput. Biol. Med.* , 108557.
- Reynaud, H., Vlontzos, A., Hou, B., Beqiri, A., Leeson, P., Kainz, B., 2021. Ultrasound video transformers for cardiac ejection fraction estimation, in: *Med. Image Comput. Comput. Assist. Interv.–MICCAI 2021: 24th International Conference, Strasbourg, France, September 27–October 1, 2021, Proceedings, Part VI 24*, Springer. pp. 495–505.
- Russakovsky, O., Deng, J., Su, H., Krause, J., Satheesh, S., Ma, S., Huang, Z., Karpathy, A., Khosla, A., Bernstein, M., et al., 2015. ImageNet large scale visual recognition challenge. *Int. J. Comput. Vis.* 115, 211–252. doi:<https://doi.org/10.1007/s11263-015-0816-y>.
- Schmid, P.J., 2010. Dynamic mode decomposition of numerical and experimental data. *J. Fluid Mech.* 656, 5–28.
- Sirovich, L., 1987. Turbulence and the dynamics of coherent structures. i. coherent structures. *Q. Appl. Math.* 45, 561–571.
- Touvron, H., Cord, M., Douze, M., Massa, F., Sablayrolles, A., Jégou, H., 2021. Training data-efficient image transformers & distillation through attention, in: *Int. Conf. Mach. Learn.*, PMLR. pp. 10347–10357.
- Tucker, L.R., 1966. Some mathematical notes on three-mode factor analysis. *Psychometrika* 31, 279–311.
- Valsaraj, A., Kalmady, S.V., Sharma, V., Frost, M., Sun, W., Sepehrvand, N., Ong, M., Equilbec, C., Dyck, J.R., Anderson, T., et al., 2023. Development and validation of echocardiography-based machine-learning models to predict mortality. *EBioMedicine* 90.

Vega, J.M., Le Clainche, S., 2021. Higher order dynamic mode decomposition, in: Vega, J.M., Le Clainche, S. (Eds.), Higher Order Dynamic Mode Decomposition and Its Applications. Academic Press, pp. 29–83. doi:<https://doi.org/10.1016/B978-0-12-819743-1.00009-4>.

World Health Organization, 1999. Cardiovascular diseases (CVDs). URL: [https://www.who.int/news-room/fact-sheets/detail/cardiovascular-diseases-\(cvds\)](https://www.who.int/news-room/fact-sheets/detail/cardiovascular-diseases-(cvds)).

Zhang, J., Gajjala, S., Agrawal, P., Tison, G.H., Hallock, L.A., Beussink-Nelson, L., Lassen, M.H., Fan, E., Aras, M.A., Jordan, C., et al., 2018. Fully automated echocardiogram interpretation in clinical practice: feasibility and diagnostic accuracy. *Circ.* 138, 1623–1635.